

Gaussian beam depth migration for anisotropic media

Tariq Alkhalifah

ABSTRACT

Gaussian beam migration (GBM), as it is implemented today, efficiently handles isotropic inhomogeneous media. The approach is based on the solution of the wave equation in ray-centered coordinates. Here, I extend the method to work for 2-D migration in generally anisotropic inhomogeneous media. Extension of the Gaussian-beam method from isotropic to anisotropic media involves modification of the kinematics and dynamics in the required ray tracing. While the accuracy of the paraxial expansion for anisotropic media is comparable to that for isotropic media, ray tracing in anisotropic media is much slower than that in isotropic media. However, because ray tracing is just a small portion of the computation in GBM, the increased computational effort in general anisotropic GBM is typically only about 40 percent. Application of this method to synthetic examples shows successful migration in layered, transversely isotropic media for reflector dips up to and beyond 90 degrees. Also, tests with synthetic data show that the quality of anisotropic migration results for a medium with velocity increasing with depth is much more sensitive to the Thomsen anisotropy parameter ϵ than to the parameter δ . Thus, a good estimate of ϵ is needed in order to apply anisotropic migration with confidence.

INTRODUCTION

Although modern migration algorithms now can treat 3-D data from areas of relatively complex structure and can accommodate turning waves associated with dip beyond 90 degrees, only recently has anisotropy been taken into account. Anisotropy may cause considerable departure of traveltimes from those expected in comparable isotropic media. Such departures will influence the accuracy of both migration and velocity analysis. For some transversely isotropic (TI) media, for example, large position errors could arise for steep reflectors when anisotropy is ignored in poststack migration (Larner and Cohen, 1993; Alkhalifah and Larner, 1994).

Migration algorithms for special cases of anisotropy have been developed in the past few years. Verwest (1989) developed a seismic migration algorithm for elliptically

anisotropic media; however, this type of anisotropy is usually a poor approximation for P-waves. Uren, Gardner and McDonald (1990) found a migrator equation for anisotropic homogeneous media that works in the frequency-wavenumber (f-k) domain. However, that approach requires that analytical expressions for the phase velocity be solved for angle of the plane-wave propagation direction; such expressions for anisotropic media are rather complicated.

Gaussian beam migration (GBM) has emerged in the past few years as a desirable method for subsurface imaging (Hale and Witte, 1992). Among its features are acceptable computational efficiency, robustness with respect to ray caustics and shadows, the ability to image reflector dips greater than 90 degrees with turning waves, and straightforward extensions for migration of nonzero-offset sections and 3-D data (Hill, 1990; Hale, 1992).

For a couple of reasons, Gaussian beam migration is particularly suited for anisotropic media. Primarily, the relatively small amount of ray tracing needed to perform Gaussian beam migration minimizes the incremental cost in modifying the algorithm for anisotropic media. Second, the method can readily handle caustics that are associated specifically with anisotropic media, such as, for example, SV-wave caustics that arise even in homogeneous media. Also, the Gaussian beam method can readily treat data from general inhomogeneous and anisotropic media with any reflector orientation.

Here, I modify the isotropic Gaussian beam migration to handle general anisotropic media in 2-D. The modification is based on anisotropic kinematic and dynamic ray-tracing. I show impulse responses for homogeneous and layered media, as well as successful migrations of synthetic data from inhomogeneous media. I also examine the relative influence of each of Thomsen's (1986) anisotropy parameters, δ and ϵ , on migration for transversely isotropic (TI) media.

GAUSSIAN BEAM MIGRATION

First, let us review Gaussian beam migration, concentrating on the aspects that pertain most to the extension to anisotropic media. Detailed description of Gaussian beam ray tracing and migration can be found in Červený and Pšenčík (1984), Hanyga (1986), Hill (1991), and Hale (1992). Here, ray propagation and polarization will be constrained to the 2-D plane. Extension to 3-D is straight forward since the general ray-tracing equations of Červený (1972) and Hanyga (1986) were actually developed for general anisotropy in 3-D.

Migration equations

In Gaussian beam migration, one first subdivides a common-midpoint (CMP) stack section into overlapping subsets of stacked traces. The stacked traces within each subset are then multiplied by a centered Gaussian taper function over midpoint.

These windowed data are then slant stacked to form beams in a range of directions characterized by different ray parameters (Hale, 1992).

The subsurface image $h_j(x, z)$ for a single beam denoted by the subscript j , at a position described by lateral position x and depth z , is calculated in GBM using the following equation (Hale, 1992):

$$h_j(x, z) = \int dp_x \left[A_R \tilde{b}(\tau_R, \tau_I) - A_I \tilde{b}_H(\tau_R, \tau_I) \right], \quad (1)$$

where \tilde{b} is a local slant stack of the Gaussian-windowed surface seismic data, and \tilde{b}_H is its Hilbert transform. A_R and A_I are the real and imaginary parts of the complex-valued amplitude, and τ_R and τ_I are the real and imaginary parts of the complex-valued time, both calculated by Gaussian beam ray tracing. p_x is the ray parameter, and \tilde{b} is calculated using

$$\tilde{b}(\tau_R, \tau_I) = \frac{1}{2\pi} \int d\omega e^{-i\omega\tau_R} e^{|\omega|\tau_I} B_j(\omega, p_x), \quad (2)$$

where $B_j(\omega, p_x)$ is the local slant stack of the surface seismic data in the frequency (ω) domain, given by

$$B_j(\omega, p_x) = \frac{|\omega|}{2\pi} F(\omega, k_x = \omega p_x),$$

and $F(\omega, k_x)$ is the 2-D Fourier transform of $f(x, t)$, the seismic data recorded at the surface $z = 0$.

In the algorithm of Hale (1992), the critical loop needed to perform GBM is as follows:

Gaussian beam migration:

```

for all points (x, z) {
    g(x, z) = 0
}

for all x_j = jΔ (all beam center locations) {
    compute f_j(t, x) by shifting and tapering data f(t, x)
    compute filtered slant stack b_j(τ, p_x) of f_j(t, x)
    for all p_x (all reflection slopes) {
        for all points (x, z) within beam {
            compute complex-valued τ_j(p_x, x, z) and A_j(p_x, x, z)
            accumulate contribution to g(x, z) from b_j(τ, p_x)
        }
    }
}

```

Here, $\tau_j(p_x, x, z)$ and $A_j(p_x, x, z)$ are the complex-valued time and amplitude, given by

$$\begin{aligned}\tau &= \tau_R + i \operatorname{sgn}(\omega)\tau_I \\ A &= A_R + i \operatorname{sgn}(\omega)A_I,\end{aligned}$$

and Δ is the spacing between the beam center locations x_j . Extension to anisotropic media requires calculating the complex-valued time and amplitude using anisotropic ray tracing.

Anisotropic kinematic ray-tracing

Červený(1972) has derived an efficient ray-tracing system in general inhomogeneous, anisotropic media. This system is based on solving for the partial derivatives of the eigenvalues for the Christoffel 3×3 matrix, Γ , rather than solving for the eigenvalues themselves. The components of this matrix are given by

$$\Gamma_{ik}(x_s, p_i) = a_{ijkl}(x_s)p_j p_l,$$

with

$$\begin{aligned}p_i &= \frac{\partial \tau}{\partial x_i}, \\ a_{ijkl} &= c_{ijkl}/\rho,\end{aligned}$$

where p_i are the components of the phase vector ($p_1 = p_x$), τ is the travelttime along the ray, ρ is bulk density, x_s are the cartesian coordinates for position along the ray, $s=1,2,3$, and c_{ijkl} are elastic coefficients, in general, functions of x_s .

From Červený (1972), the ray-tracing system for general inhomogeneous anisotropic media is given by

$$\begin{aligned}\frac{dx_i}{d\tau} &= a_{ijk}p_l g_j g_k, \\ \frac{dp_i}{d\tau} &= -\frac{1}{2} \frac{\partial a_{njk}}{\partial x_i} p_n p_l g_j g_k,\end{aligned}$$

where g_i are the components of the eigenvector \mathbf{g} (the direction of particle motion).

In 2-D, all out-the-plane components are eliminated, namely all components with subscript 2. The eigenvectors are then calculated as follows.

$$\begin{aligned}g_1 g_1 &= \frac{\Gamma_{33} - G}{\Gamma_{11} + \Gamma_{33} - 2G}, \\ g_3 g_3 &= \frac{\Gamma_{11} - G}{\Gamma_{11} + \Gamma_{33} - 2G},\end{aligned}$$

and

$$g_1 g_3 = \frac{-\Gamma_{13}}{\Gamma_{11} + \Gamma_{33} - 2G},$$

where G is the eikonal, described below, and $G = 1$ along the ray.

Because the square-roots associated with calculation of the phase and group velocities directly from the eikonal, G_m , have been eliminated, this is a relatively efficient method of ray tracing, especially in general anisotropic media.

Anisotropic dynamic ray-tracing

The parameters p and q , which relate a calculated central ray to a nearby projected paraxial ray, are given by Červený (1981) for isotropic media

$$\frac{dq}{d\tau} = v^2 p \quad \frac{dp}{d\tau} = -\frac{v_{,nn}}{v} q,$$

where n is the normal to the ray direction (which is the same as phase direction for isotropic media), and v and $v_{,nn}$ are, respectively, the velocity and its second derivative with respect to n .

A paraxial ray is a ray (not actually traced) in the vicinity of the central ray. Its normal distance from the central ray is described by the value of q , and the difference in the two propagation angles is characterized by p .

For anisotropic media, the dynamic ray tracing is more complicated. The ray-centered coordinates are no longer orthogonal as they are for isotropic media, so we must compute an extra quantity, V , along the ray to compensate for non-orthogonality. The dynamic ray-tracing equations given by Hanyga (1986) for anisotropic media are

$$\frac{dq}{d\tau} = Mp + Vq$$

and

$$\frac{dp}{d\tau} = -Vp - Hq,$$

where M, V, H are derivatives of the eikonal with respect to n and p_n , the ray parameter in the direction of n , normal to the phase direction. These derivatives are given by

$$\begin{aligned} M &= 0.5 \frac{\partial^2 G_m}{\partial n^2} - 0.25 \left(\frac{\partial G_m}{\partial n} \right)^2 \\ H &= 0.5 \frac{\partial^2 G_m}{\partial p_n^2} - 0.25 \left(\frac{\partial G_m}{\partial p_n} \right)^2 \\ V &= 0.5 \frac{\partial^2 G_m}{\partial p_n \partial n} - 0.25 \frac{\partial G_m}{\partial p_n} \frac{\partial G_m}{\partial n}. \end{aligned}$$

Here, G_m , $m=1,2,3$ are the eigenvalues of the Christoffel equation

$$\text{Det}(\Gamma_{jk} - G_m \delta_{jk}) = 0.$$

G_m are the three eigenvalues representing the eikonal equation for the three wave types: quasi P-wave when $m=1$; quasi SV-wave when $m=2$; and quasi SH-wave when $m=3$. G_m for anisotropic media is given by

$$G_m = a_{ijkl} p_i p_l g_j g_k.$$

Paraxial expansion

Consider ray-centered coordinates (s, n) , where s is distance along the ray and n is the distance normal to the phase-velocity direction. The expansion of traveltime along n using Taylor's series gives the parabolic equation (Červený, 1981)

$$T(s, n) \cong T(s) + 0.5 \frac{\partial^2 T(s)}{\partial n^2} n^2. \quad (3)$$

$\frac{\partial^2 T(s)}{\partial n^2}$ is a complex variable for Gaussian beam ray-tracing given by (Červený and Pšenčík, 1984)

$$\frac{\partial^2 T(s)}{\partial n^2} = \frac{p_1 + ip_2}{q_1 + iq_2},$$

where q_1, p_1 and q_2, p_2 are solutions of the dynamic ray-tracing for a plane source and a point source, respectively. The real part of this complex-valued term describes ray curvature, and the imaginary part is a factor associated with the Gaussian-shaped decay away from the ray.

This is the same equation used for the isotropic case; however, here n is in the direction normal to the phase direction, not to the ray direction. Furthermore, q_1, p_1, q_2 and p_2 are computed using anisotropic dynamic ray-tracing, as discussed above, where their initial values are taken to be $q_1 = 1, p_1 = 0, q_2 = 0$ and $p_2 = 1$.

Initial beam width

In equation (3), we are representing the wavefront by a sequence of parabolic expansions. Let us examine the accuracy of these expansions, especially for strong anisotropy. Figure 1 shows a point source in a homogeneous half-space, and a single ray emanating from this source. Again, s is the length along the ray, and n is the distance to the receiver in the direction of the normal to the phase-velocity direction. Although Gaussian beams are generally a combination of point and plane-wave solutions (see, e.g., Hill, 1990), for this homogeneous case the only error in the traveltime expansion at the receiver comes from the point-source contribution. Plane-wave traveltime expansions are exact in a homogeneous medium for both isotropic and anisotropic media. This is so simply because for plane waves the traveltime calculated at the receiver position is identical to that at the ray at the point of the expansion [$\text{Real}(\frac{\partial^2 T(s)}{\partial n^2})=0$]. However, this is not the case for point sources, where the wavefront is curved and approximated by equation (3), even in homogeneous media. In this test, I compare the traveltimes calculated using the parabolic expansion with the exact traveltimes.

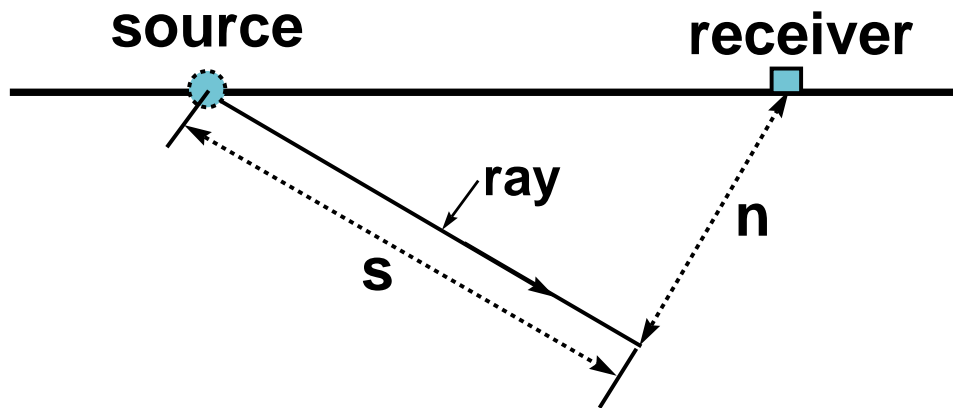


FIG. 1. Schematic vertical section illustrating the lengths s and n for a certain ray in a homogeneous medium.

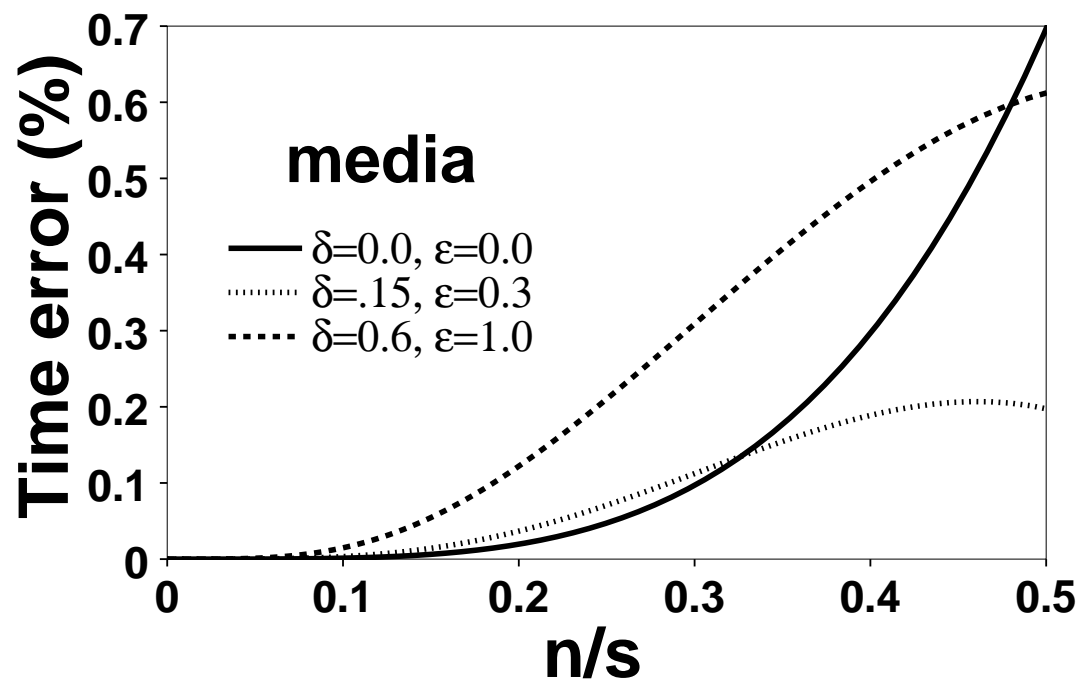


FIG. 2. Percentage time error as a function of n/s for the model shown in Figure 1.

Figure 2 shows the percent difference in those traveltimes, as a function of the ratio n/s . This ratio varies for the different rays that contribute to a given receiver position. Curves are shown for three different anisotropic media characterized by the δ and ϵ parameters of Thomsen (1986). Clearly, for low values of n/s , the errors are largest for strong anisotropy (i.e., large δ and ϵ). Overall, the errors ($\sim 0.5\%$) are small, but they indicate the limitations that the parabolic expansion has in approximating the wavefront in the presence of strong anisotropy.

Figure 3 shows the actual expansion of the different beams contributing to the same receiver for an isotropic medium and for strongly anisotropic one. The location of our receiver is in a slightly more complicated (i.e. more highly curved) part of the wavefront for the strongly anisotropic medium. Interestingly, Figure 3 shows that the amplitude decay away from the central ray is greater for the anisotropic medium than it is for the isotropic medium. We can get a sense of what is happening by observing the example in Figure 4a. Figure 4a shows migration impulse responses for P-waves in a strongly anisotropic, homogeneous medium. The anisotropy accounts for the departure in shape of the impulse response from the familiar circular shape in isotropic media. For this case the beam width is smallest near vertical, where the wavefront has the highest curvature. In addition, the largest concentration of rays occurs in the portions of the wavefront with highest curvature. In contrast, for the smoother parts, near 45-degree ray propagation, the beam width is much broader, and the wavefront is characterized by relatively few rays. It then happens that, although in GBM the number of rays generated to calculate the wavefield may be the same for both isotropic and anisotropic media, the angular distribution of the rays differ.

With a proper choice of initial beam width, the beam width along the ray will not expand to large values of n/s . Here, I compute the initial beam width using the same equation used by Hill (1990)

$$w_0 = \frac{v_{avg}}{f_{min}},$$

where f_{min} is the minimum frequency and v_{avg} is the average of the horizontal and vertical velocities over the entire grid.

Ray-parameter spacing

For isotropic media, Hale (1992) uses as the ray-parameter increment

$$(\Delta p_x)_{iso} = \frac{2\pi}{3l\sqrt{|\omega_l\omega_h|}},$$

where ω_l is the lowest frequency of interest, ω_h is the highest; and l is the related initial beam width. This choice ensures adequate ray coverage to avoid aliasing and, therefore, to properly construct the wavefield. For anisotropic media, the values of p_{min} and p_{max} are different than those for isotropic media, given the same minimum

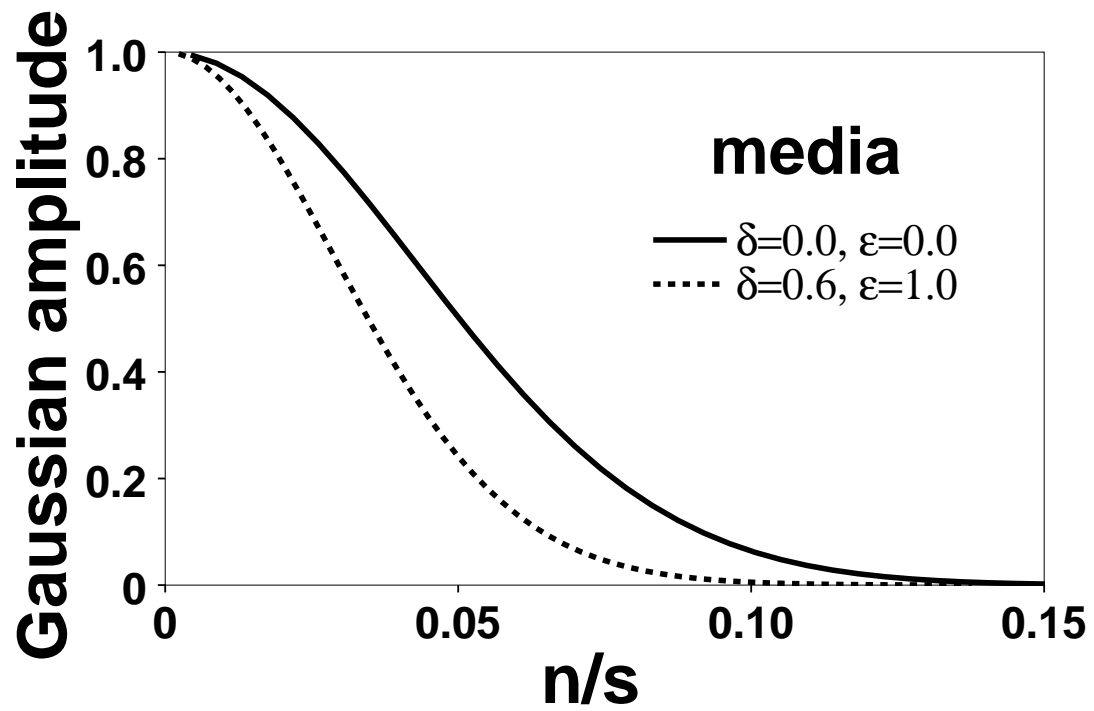


FIG. 3. Gaussian weighting away from the ray, as a function of n/s .

and maximum angles of interest. As a result, the following modified expression yields the appropriate amount of ray coverage.

$$\Delta p_x = (\Delta p_x)_{iso} \frac{2v_{min}}{V_{min}(p_{max}) + V_{min}(p_{min})},$$

where v_{min} is the minimum vertical velocity at the surface ($z = 0$), and $V_{min}(p_{max})$ and $V_{min}(p_{min})$ are the phase velocities corresponding to the maximum and minimum ray parameters at the point where vertical velocity $V_p = v_{min}$. Recall that ray angles differ from phase angles in anisotropic media, a fact that must be taken into consideration when determining the minimum and maximum ray parameter of interest. In anisotropic media, for each initial ray parameter p_x , I solve for the phase angle θ using

$$p_z = \sqrt{\frac{1}{V^2(\theta)} - p_x^2},$$

where p_z is the horizontal ray parameter ($p_z = p_3$), and $V(\theta)$ is the phase velocity. For general anisotropy, this turns out to be a quartic equation, which I solve by the secant method. For transversely isotropic media, however, the equation reduces to a quadratic.

MIGRATION COST

P-wave ray-tracing in a general anisotropic inhomogeneous medium is a much slower process than that in an isotropic medium. One reason is that ray tracing in anisotropic 2-D media requires six velocity fields, corresponding to the six position-variant elastic coefficients, whereas ray tracing in isotropic media requires only one velocity field. A second and more important reason is that ray tracing in anisotropic media involves much more complicated and more computationally extensive equations than does that in isotropic media. However, isotropic ray tracing constitutes only about 2 percent of the cost of GBM for generally inhomogeneous models. Therefore, the substantially increased cost of ray tracing in anisotropic media raises the computation cost of the full GBM process by only a modest amount—generally by no more than 40 percent. This speed characteristic is not shared by Kirchhoff migration. For that method, ray tracing constitutes the major portion of the processing, so Kirchhoff migration must bear the full additional cost of ray tracing in general, anisotropic media.

In addition to its speed advantage for anisotropic migration, GBM can handle caustics and migrate accurately all P-wave arrivals (not only first arrivals). In contrast, Kirchhoff migration has serious problems in handling caustics, a common occurrence when migrating S-waves in anisotropic media.

The 40-percent difference in computation cost between isotropic and anisotropic GBM holds for general anisotropic, inhomogeneous 2-D media. When considering only TI media or factorized TI media the cost difference reduces substantially, to about 10 percent.

SYNTHETIC EXAMPLES

The changes mentioned above do not limit GBM in any way. Specifically, it is still extendable to 3-D, and its efficiency is largely unchanged; relative to the cost of the migration, the cost of computing τ and A for anisotropic media is small.

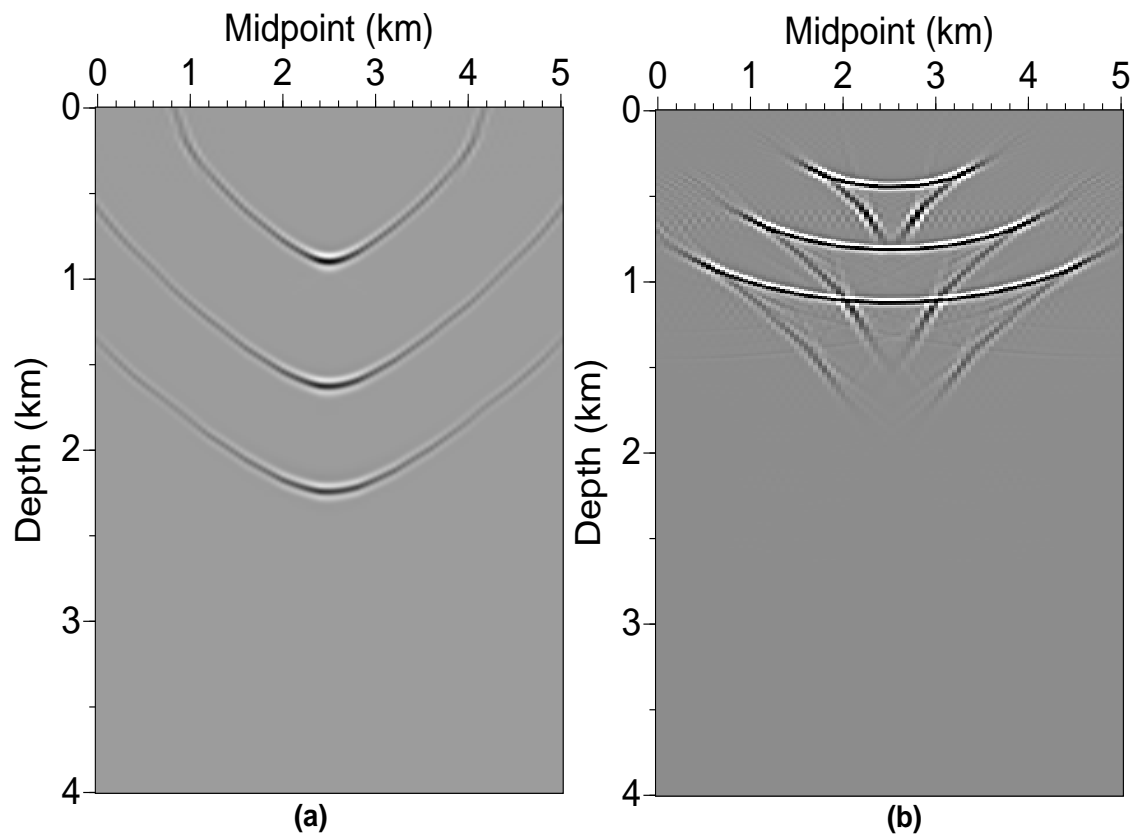


FIG. 4. GBM impulse responses for (a) P-wave, and (b) SV-wave in homogeneous weathered gypsum ($\delta = -0.14$, $\epsilon = 1.1$) with vertical axis of symmetry.

Smooth media

Figure 4 shows the response of GBM to impulses at times 0.8, 1.6, and 2.3 s, with a constant vertical P-wave velocity of 2000 m/s and constant vertical S-wave velocity of 1000 m/s for (a) P-waves, and (b) S-waves, in the weathered-gypsum TI medium of Thomsen (1986). This medium has Thomsen anisotropy parameters $\delta = -0.14$ and $\epsilon = 1.1$. As mentioned above, the wavefronts (and amplitudes along wavefronts) here are very different from the circular ones of an isotropic medium, especially for the SV-wave with its obvious triplication (caustics), which is handled without difficulty by the Gaussian beam migration.

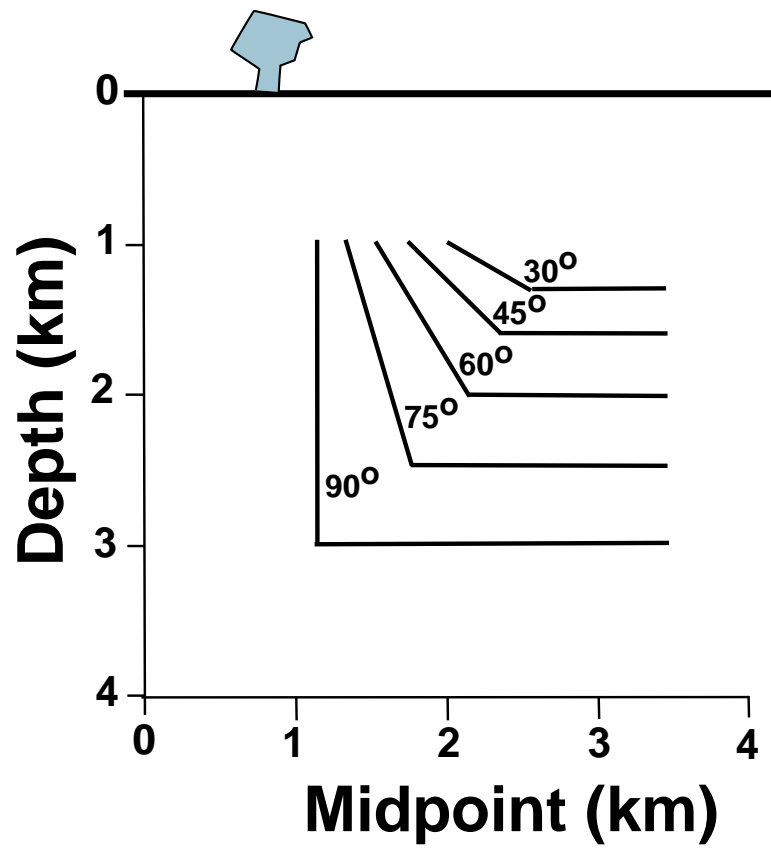


FIG. 5. Model of reflectors with dips of 0, 30, 45, 60, 75, 90 degrees. Note that the vertical reflector is at 1.2-km midpoint position.

Now, consider the depth model shown in Figure 5. It consists of five reflectors, each of which has a horizontal segment and a dipping one. Figure 6 shows synthetic zero-offset sections for this model in (a) an isotropic medium, and (b) an interbedded shale-limestone TI medium, with anisotropy parameters $\delta = 0.0$, $\epsilon = 0.134$, both with vertical velocity $v(z) = 3000 + 0.5z$ m/s. Figure 6a was generated using a Kirchhoff modeling program for an isotropic medium with a linear velocity increase with depth. Figure 6b was generated using a modified version of that modeling program that treats factorized transversely isotropic (FTI) media (Alkhalifah, 1994), i.e., media for which δ and ϵ are independent of position. The dot shown in both figures is for reference in comparing the positions of the reflection from the vertical reflector for the isotropic and TI media.

Figure 7 shows migrations of the data in Figure 6b using (a) standard, isotropic GBM and (b) GBM modified for anisotropic media. The velocity used to derive medium velocities for the standard GBM is the best-fit stacking velocity for horizontal reflectors, whereas the correct medium parameters are used in the anisotropic GBM. Clearly the image in Figure 7b is superior to that in Figure 7a. The image from migration that ignores anisotropy, Figure 7a, not only is undermigrated, it is placed at too great a depth because stacking velocity exceeds the vertical root-mean-square (rms) velocity. This depth error is of the sort described by Banik (1984), Winterstein (1986), and Verwest (1989). In contrast, the reflector locations have been correctly imaged by the modified GBM, Figure 7b. Here, because I use a simple version of the anisotropic GBM that considers only FTI media, the computation cost difference between the isotropic and anisotropic GBM is less than 10 percent.

Figure 8 shows isotropic GBM and anisotropic GBM for the Cotton Valley shale medium of Thomsen (1986), with anisotropy parameters $\delta = 0.205$, $\epsilon = 0.135$, and vertical velocity $v(z) = 3000 + 0.5z$ m/s. Following Larner and Cohen (1992), I used the best-fit stacking velocity (for horizontal reflectors) to minimize the lateral position errors. The isotropic GBM not only yielded a considerably overmigrated image, it again resulted in large vertical shifts in the reflector position. As before, the depth error in effect is caused by using the wrong velocity, namely stacking velocity in a TI medium, for the vertical travelttime-to-depth conversion.

For both anisotropic media — shale-limestone and Cotton Valley shale — the anisotropic GBM (with the correct anisotropy parameters) gave a substantially better image of the reflector position than did the GBM that ignores anisotropy.

Layered media

As in other high-frequency approximations, accuracy in the ray tracing for GBM requires some degree of smoothing of the input velocity field. For general anisotropic media, smoothing must be applied to all six needed velocity fields. If any of the velocity fields contains sharp velocity discontinuities, the quality of the migrated image will be degraded, the degree of this degradation depending on the sizes and locations of the discontinuities.

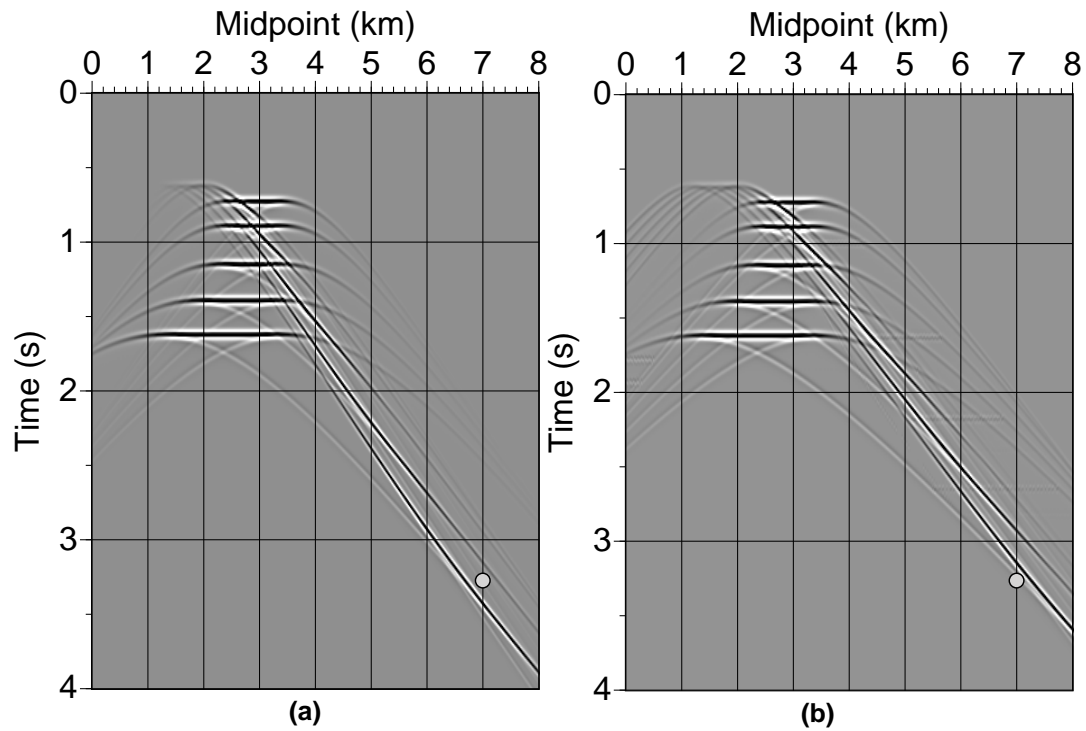


FIG. 6. Synthetic zero-offset seismograms for the structural model in Figure 5, for (a) an isotropic medium, and (b) a shale-limestone, transversely-isotropic medium. Both media have vertical velocity $v(z) = 3000 + 0.5z$ m/s, and reflector dips ranging from 0 to 90 degrees.

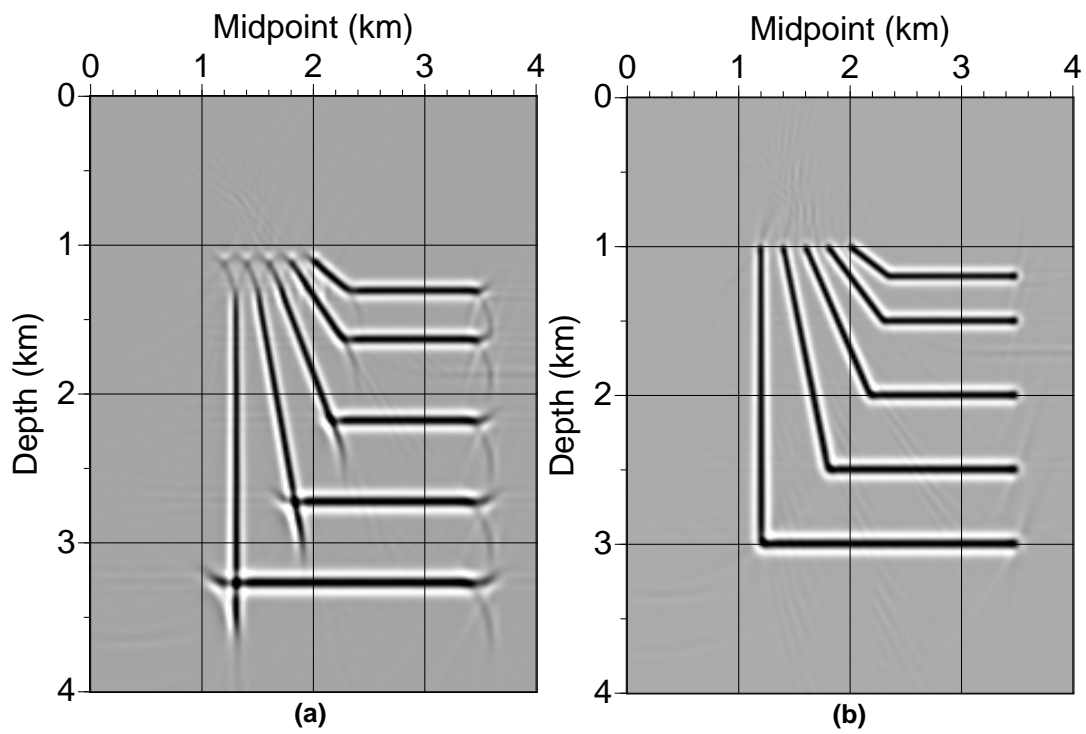


FIG. 7. Migration of the data in Figure 6b using (a) the isotropic GBM algorithm, and (b) anisotropic GBM, for the shale-limestone TI medium.

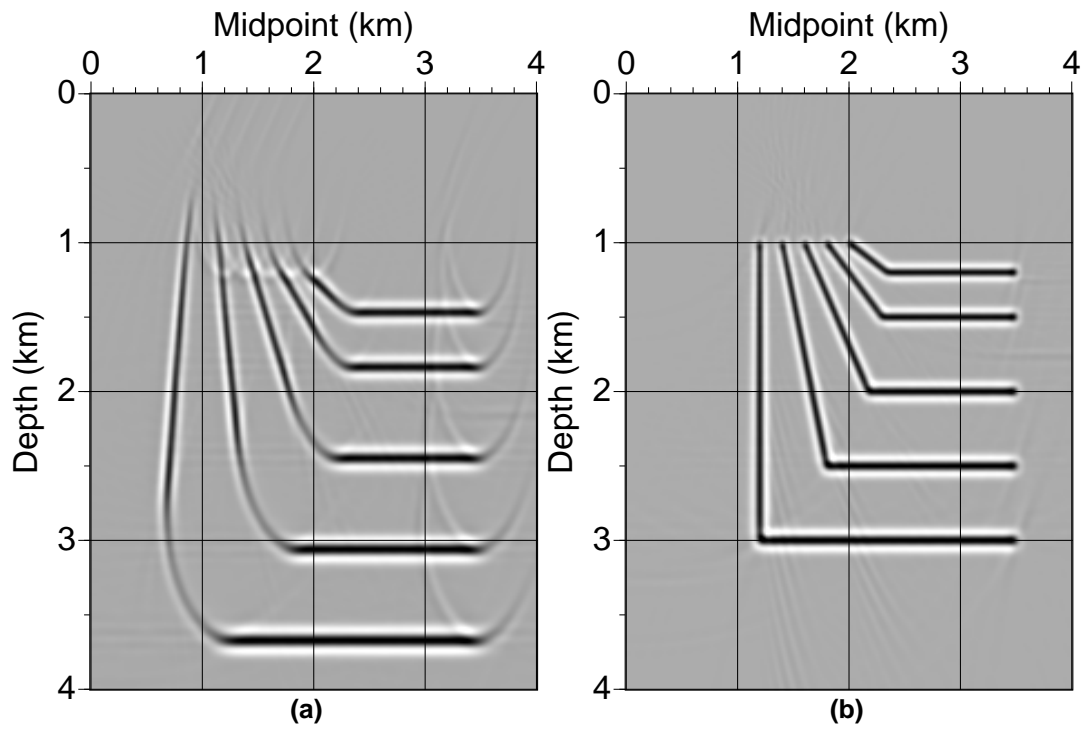


FIG. 8. Migration of data from the structural model shown in Figure 3 for Cotton Valley shale with $v(z) = 3000 + 0.5z$ m/s, using (a) isotropic GBM, and (b) anisotropic GBM.

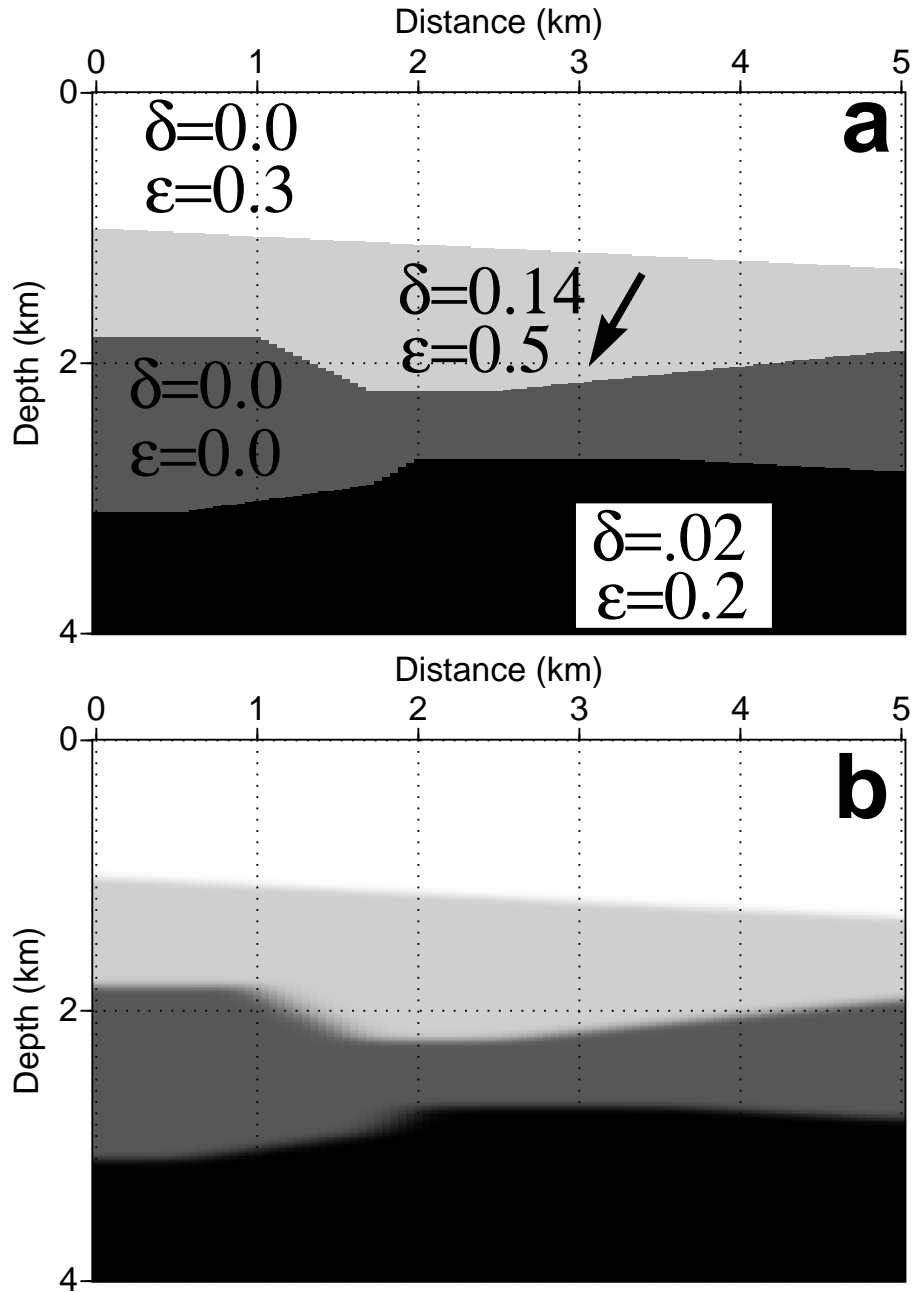


FIG. 9. (a) Model containing layers with different anisotropy parameters in each layer. All layers have vertical symmetry axis with the exception of the second layer where the symmetry axis is in the direction of the arrow. From top layer to bottom, the vertical velocity is 1.0 km/s, 1.5 km/s, 2.5 km/s, and 3.0 km/s. (b) Smoothed version of the above model.

Figure 9a shows a model of four homogeneous, transversely isotropic layers, with different anisotropy parameters in each layer. The vertical velocity is indicated by the shading level; the vertical velocity in the first layer is 1 km/s, and in the bottom layer, 3 km/s. For both these media, the axis of symmetry is vertical. The arrow direction in the second layer corresponds to the symmetry-axis direction, tilted by 30 degrees from the vertical. Figure 9b shows a smoothed version of the model. Although the smoothing is shown here for the vertical velocity, all needed velocity fields (corresponding to the elastic coefficients) are smoothed to the same degree. For the smoothing, the velocity field was convolved with a two-dimensional, Gaussian-shaped, point-spread function. Here, the width of the Gaussian function (the half-amplitude point) was 0.1 km in all directions.

Figure 10a shows the impulse response, for the model in Figure 9a, for input pulses at three different times, all located at common-midpoint position 2.5 km. Figure 10b shows the corresponding impulse responses for the smoothed model in Figure 9b.

The importance of the velocity smoothing is evident from comparison of these two sections. Especially, here where the discontinuities are large, the impulse responses are obliterated for the unsmoothed model, a striking shortcoming of the high-frequency approximation in such a complex structural model. Clearly, the impulse responses associated with the smoothed model are much better. Note that for impulses in and beneath the second layer, where the symmetry axis is tilted, the impulse responses in Figure 10b are also tilted.

SENSITIVITY TO δ VERSUS SENSITIVITY TO ϵ

For transversely isotropic media, as shown by Alkhalifah and Larner (1994), only the two parameters δ and ϵ influence the anisotropic aspects of the migration output for a given $v(z)$ medium.

Figure 11 shows a migration for the Mesaverde shale FTI medium with vertical axis of symmetry, where turning waves were needed to image the overturned portion of the reflector. Mesaverde shale has anisotropy parameters $\delta = 0.078$ and $\epsilon = 0.128$, and this model has a vertical velocity $v(z) = 2000 + 0.8z$ m/s.

Migrating the model in Figure 11a using inaccurate values of δ and ϵ gives an idea of the relative influence that these parameters have on the quality of the imaged section. Figure 12a shows a migration of the model in Figure 11a using a δ value of 0.0 instead of the correct value of 0.078. With this erroneous choice of parameter, the image is inconsequentially different from that shown in Figure 11b. On the other hand, distorting the value of ϵ by the same amount as δ , causes the migrated image to become highly inaccurate (Figure 12b). Thus, here, ϵ has a greater influence on the accuracy of the migrated section than does δ . These results exemplify the conclusions given by Alkhalifah and Larner (1994); i.e., where velocity increases with depth and when doing migration with an algorithm that honors anisotropy, the parameter ϵ is much more important than is δ in governing the accuracy of the migration. Stated

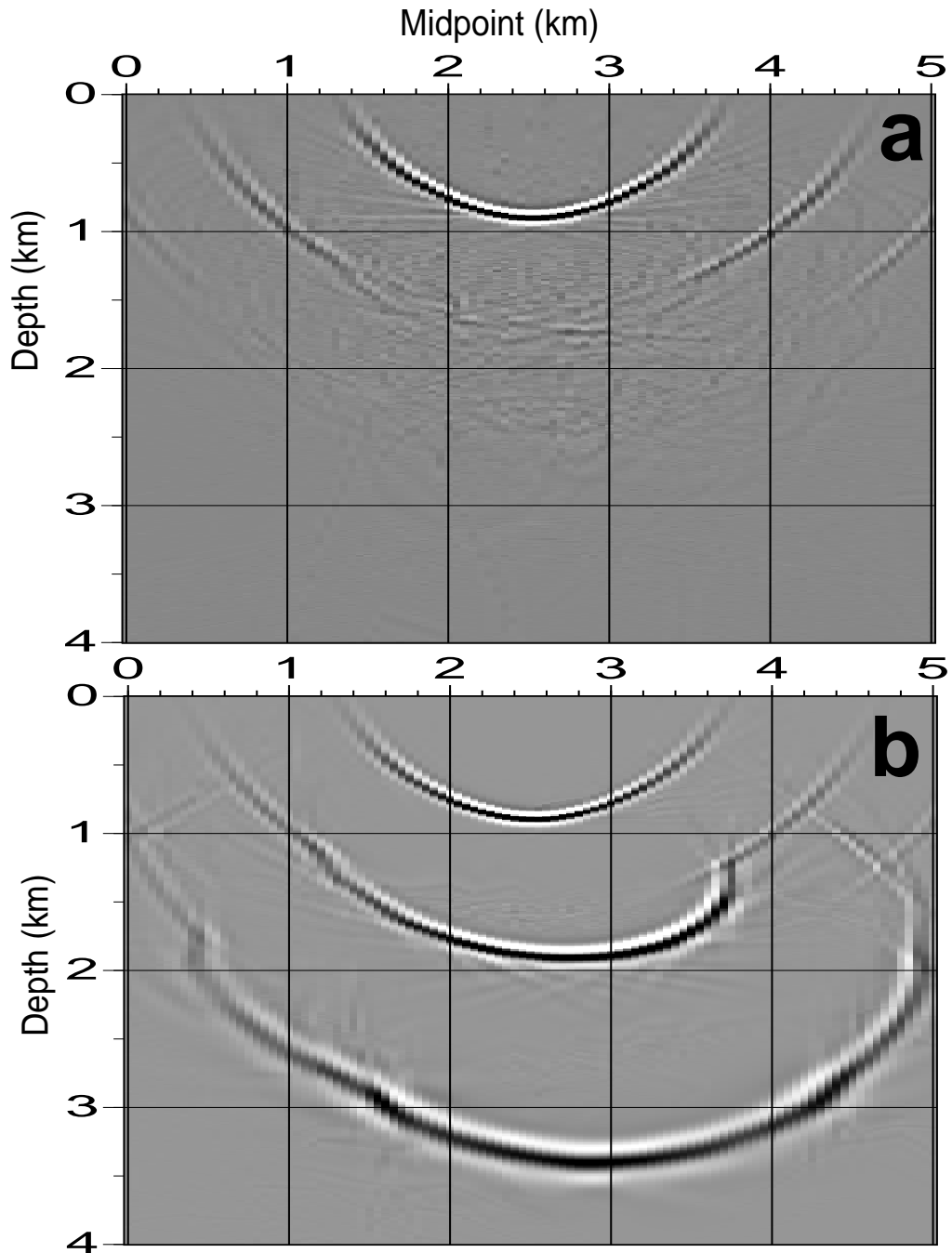


FIG. 10. (a) GBM impulse responses for the model in Figure 9a. (b) GBM impulse responses for the smoothed model in Figure 10a.

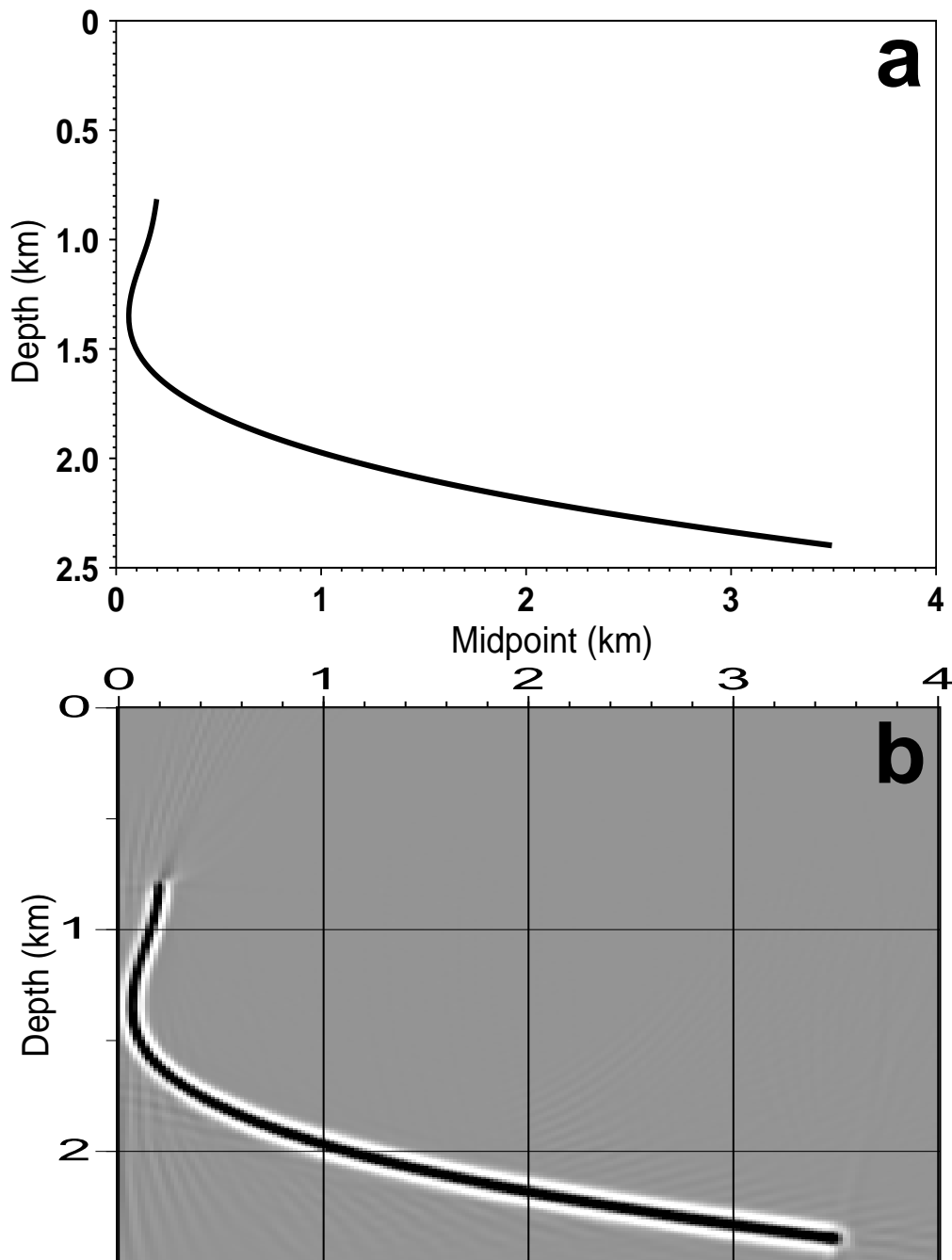


FIG. 11. (a) Model containing reflector with dip as large as 120 degrees. (b) Anisotropic GBM of data from the above structural model for Mesaverde shale, with vertical velocity $v(z) = 3000 + 0.8z$ m/s.

differently, the parameter that must be estimated with greater accuracy is ϵ . This result does not diminish the importance of δ in estimating the vertical velocity, which is critically important to reducing any possible depth errors.

CONCLUSION

Because of the sensitivity of migration to velocity, anisotropy could have a large influence on the accuracy of migrated images. Use of the modified GBM with correct velocity information can substantially reduce errors that arise when anisotropy is ignored, and thus provide improved images. Modified GBM, like standard GBM, can be extended to 3-D by simply using the 3-D version of dynamic and kinematic ray tracing, combined with application of beam expansions in 3-D.

The Gaussian beam migration for anisotropic media developed here is both efficient and general: efficient in that it is slower than its isotropic counterpart by only 40 percent, and general in that it can handle arbitrary (but velocity-smoothed) inhomogeneous media. In principle, the method works for any strength of anisotropy; it handles caustics; and it migrates all P-wave arrivals. The efficiency is particularly important when using this program to estimate anisotropy parameters, where the migration algorithm typically must be exercised repeatedly.

Clearly, it is important to estimate all anisotropy parameters. However, as shown here, for media with velocity increasing with depth, it is most important that ϵ be accurately estimated; the parameter δ has less influence on the accuracy of migration.

ACKNOWLEDGMENTS

I thank Professor Ken Larner for his critical input and review of the paper. Thanks are due to the Center for Wave Phenomena, Colorado School of Mines, for its technical support, and also to KACST, Saudi Arabia, for its financial support. Financial support for this work also was provided in part by the United States Department of Energy, (this support does not constitute an endorsement by DOE of the views expressed in this paper) and by the members of the Consortium Project on Seismic Inverse Methods for Complex Structures at the Center for Wave Phenomena, Colorado School of Mines.

REFERENCES

- Alkhalifah, T., 1994, Efficient modeling in transversely isotropic, inhomogeneous media: Submitted to Geophysics.
- Alkhalifah, T., and Larner, K., 1994, Migration errors in transversely isotropic media: Submitted to Geophysics.
- Banik, N.C., 1984, Velocity anisotropy of shales and depth estimation in the North Sea basin: Geophysics, **49**, 1411-1419.

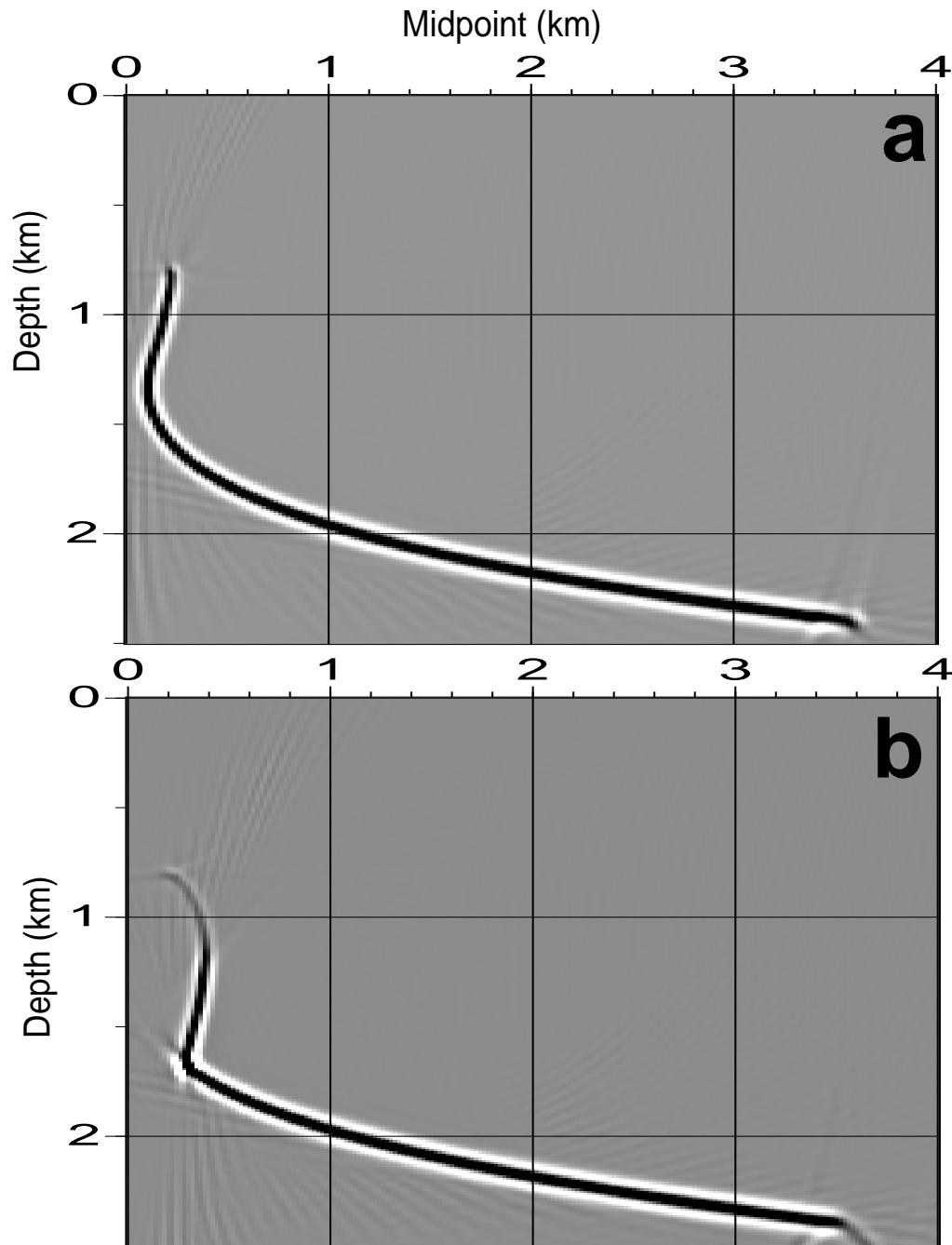


FIG. 12. (a) Anisotropic GBM of data from the structural model in Figure 11a for Mesaverde shale using a δ value of 0.0 instead of the true value $\delta = 0.078$. (b) Anisotropic GBM of data from the same model for Mesaverde shale using an ϵ value of 0.05 instead of the true value $\epsilon = 0.128$.

- Červený, V., 1972, Seismic rays and ray intensities in inhomogeneous anisotropic media: *Geophys. J. R. Astr. Soc.*, **29**, 1–13.
- Červený, V., 1981, Computation of geometrical spreading by dynamic ray tracing: *Stanford Exploration Project*, **28**, 49–59.
- Červený, V., and Pšenčík, I., 1984, Gaussian beams in elastic 2-D laterally varying layered structures: *Geophys. J. R. Astr. Soc.*, **78**, 65–91.
- Hale, D., 1992, Migration by the Kirchhoff, slant stack, and Gaussian beam methods: *Center of Wave Phenomena (CWP), Report 121*, Colorado School of Mines.
- Hale, D., and Witte, D., 1992, Migration: Progress and predictions: Presented at the 62nd Ann. Internat. Mtg. Soc. Expl. Geophys., Expanded Abstracts, 610–612.
- Hangya, A., 1986, Gaussian beams in anisotropic elastic media: *Geophys. J. R. Astr. Soc.*, **85**, 473–563.
- Hill, N. R., 1990, Gaussian beam migration: *Geophysics*, **55**, 1416–1428.
- Larner, K. and Cohen, J., 1993, Migration error in factorized transversely isotropic media with linear velocity variation with depth: *Geophysics*, **58**, 1454–1467.
- Thomsen, L., 1986, Weak elastic anisotropy: *Geophysics*, **51**, 1954–1966.
- Uren, N., F., Gardner, G., H., F., and McDonald, J., A., 1990, The migrator's equation for anisotropic media: *Geophysics*, **55**, 1429–1434.
- Verwest, B. J., 1989, Seismic migration in elliptically anisotropic media: *Geophysical Prospecting*, **37**, 149–166.
- Winterstein, D. F., 1986, Anisotropy effects in P-wave and S-wave stacking velocity contain information on lithology: *Geophysics*, **51**, 661–672.